Two novel magnesium(II) meso-tetraphenylporphyrin-based coordination complexes: Syntheses, combined experimental and theoretical structures elucidation, spectroscopy, photophysical properties and antibacterial activity

N. Amiri, M. Hajji, F.B. Taheur, S. Chevreux, T. Roisnel, G. Lemercier, H. Nasri

Two novel magnesium(II) *meso*-tetraphenylporphyrin-based coordination complexes: syntheses, combined experimental and theoretical structures elucidation, spectroscopy, photophysical properties and antibacterial activity.

Nesrine Amiri[a], Melek Hajji [b, *], Fadia Ben Taheur [c], Sylviane Chevreux [d], Thierry Roisnel [e], Gilles Lemercier [d] and Habib Nasri [a]

[a] *Laboratory of Physical Chemistry of Materials, University of Monastir, Avenue of the Environment, 5019 Monastir, Tunisia.*
[b] *Research Unit: Electrochemistry, Materials and Environment, University of Kairouan, 3100 Kairouan, Tunisia.*
[c] *Laboratory of Analysis, Treatment and Valorisation of Environmental Pollutants and Products, Faculty of Pharmacy, Monastir University, Tunisia.*
[d] *University of Reims Champagne-Ardenne, ICMR UMR CNRS n ° 7312, BP 1039-51687, Reims Cedex 2, France.*
[e] *University of Rennes 1, CNRS, Institute of Chemical Sciences of Rennes, UMR 6226, F-35042 Rennes Cedex, France.*

[*] *Corresponding author: E-mail address: melekhajji1989@gmail.com T: (+216) 55 36 72 81.*

Abstract Two novel magnesium(II) tetraphenylporphyrin-based six-coordinate complexes; bis(hexamethylenetetramine)(5,10,15,2O tetrakis[4(benzoyloxy)phenyl]porphinato) magnesuim(II) (**1**) and bis(1,4-diazabicyclo(2.2.2)octane) (5,10,15,2O-tetrakis[4-(benzoyloxy)phenyl]porphinato)magnesium(II) (**2**) have been synthesised and confirmed by proton nuclear magnetic resonance, mass spectrometry, elemental analysis and IR spectroscopy. Both crystal structures were determined and described by single crystal X-ray diffraction analysis and Hirshfeld surfaces computational method. All Mg(II) atoms are surrounded by four porphyrin nitrogen atoms and two axial ligands coordinated to the metal ion through one nitrogen atom, forming a regular octahedron. In both complexes, molecular structures and three-dimensional framework are stabilised by inter-and intramolecular C–H···O and C–H···N hydrogen bonds, and by weak C–H···Cg π interactions. UV-visible and Fluorescence investigations, respectively, show that studied complexes have a strong absorption in red part and exhibit an emission in the blue region. The HOMO-LUMO energy gap values, modelled using the DFT approach, indicates that both studied compounds can be classified as semiconductors. The role of these complexes as novel antibacterial agents was also performed.

Keywords: magnesium(II) tetraporphyrin coordination complexes, X-ray diffraction, Hirshfeld surfaces, DFT approach, Fluorescence, antibacterial activity.

1. Introduction

The design and synthesis of supramolecular coordination assemblies of porphyrin-based ligands complexes have received considerable attention due to their advantageous applications such as oxidation catalysts for hydroxylation of alkanes and epoxidation of alkenes [1-4], chemical sensors [5], and semi-conductors [6]… Several derivatives of porphyrin have been developed as photosensibilizating agents (PS) for photodynamic therapy (PDT) [7-9]. Recent in vitro studies demonstrated that porphyrins are also effective against viruses and yeasts [10,11]. In addition to these important roles, the porphyrinic nucleus presents an efficient source for the synthesis of a large number of active agents in the antibacterial and antimicrobial activities [12,13]. In this context, it has to be pointed out that Zn(II), Cu(II), Co(III) and Zr(IV) metalled porphyrins [14-16] possess interesting activities against several bacterial species. Ever since the metalloporphyrins were discovered, a great deal of research has been devoted to the exploration of their axial coordination and its specifications in organometallic chemistry. The interaction of metalloporphyrins with donor molecules via axial coordination either can strongly influence the photophysical properties and the efficiency of energy or electron transfer processes [17]. For a better understanding of the principles governing the structural properties of this type coordination complexes, hydrogen bonding, π–π stacking and intermolecular C–H...Cg interactions have been studied [18-20]. In continuation of our work on functionalization of *meso*-tetraarylporphyrins, we combined the porphyrin framework with two nitrogen based ligands (HTMA and DABCO) to design two new six-coordinated Mg(II) porphyrins complexes: bis(HTMA)(5,10,15,20-tetrakis[4-(benzoyloxy)phenyl] porphyrinato) magnesuim(II), with formula $[Mg^{II}(TPBP)(HTMA)_2]$ (**1**), and bis(DABCO)(5,10,15,20-tetrakis[4 (benzoyloxy)phenyl] porphyrinato)magnesuim(II), with formula $[Mg^{II}(TPBP)(DABCO)_2]$ (**2**). Both prepared complexes were characterised by X-ray diffraction, infrared, proton nuclear magnetic resonance spectroscopies, mass spectrometry, and elemental analysis. Their photophysical studies revealed S2 emission along with a characteristic S1 emission band in the case of newly prepared free-base, and magnesium porphyrins. In the light of 3D Hirshfeld surfaces [21-30] and the associated 2D fingerprint plots [31-34], a quantitative crystal structure analysis was made. The biological activity of the H_2TPBP porphyrin Mg(TPBP), free porphyrin TPBP, complexes 1 and 2 were tested against some Gram (+) (*Staphylococcus aureus*, Enterococcus faecalis) and Gram (-) (Pseudomonas aeruginosa, Escherichia coli) bacteria.

2. Experimental

2.1 Syntheses

All chemicals and reagents were purchased from SIGMA ALDRICH or ACROS ORGANICS. Used solvents were purified using the available literature methods [35]. Macrocycles of *meso*-tetrakis[4-(benzoyloxy)phenyl]porphyrin (H_2TPBP) and *meso*-tetrakis[4-(benzoyloxy)phenyl] porphyrinato)magnesuim(II) complex (Mg(TPBP)) were prepared as previously described [36-37]. Scheme S1 gives the main steps of the preparation of (**1**) and (**2**).

Synthesis of the meso-tetrakis[4-(benzoyloxy) phenyl] porphyrin (H_2TPBP): 4-formylphenylbenzoate (500 mg, 2.21 mmol), and pyrrole (153 µL, 2.21 mmol) were added to distilled chloroform (300 mL) in a double necked round bottom flask under argon and shielded from light. Boron trifluoride diethyl etherate, $BF_3.OEt_2$ (192.4 µL) was added, and the reaction was kept at room temperature for two hours. Two pipettes of triethylamine and 0.75 equivalents of p-chloranil (179.2 mg, 1.66 mmol) were added and the solution was heated to reflux (light protection was removed). After 1 hour, obtained solution was cooled to room temperature. Solvent was evaporated and the residue was filtered over silica with $CHCl_3$/hexane/ (1 : 9). Expected compound was obtained as a purple solid (yield 57%). ^{1}H NMR [300 MHz, $CDCl_3$] δ(ppm) 8.94 (s, 8H, Hβ-pyrrol), 8.42 (d, 8H, *J*=7.5 Hz), 8.33 (d, 8H, *J*=7.6 Hz), 7.71 (d, 8H, *J*=7.5 Hz), 7.62 (m, 12H), -2.80 (s, 2H, Hpyrrol). UV/vis [λ_{max} (nm) in CH_2Cl_2, (log ε)]: 419 (5.90), 514 (4.46), 551 (4.13), 590 (3.94), 646 (3.84). MS [ESI]: m/z calcd for $C_{72}H_{46}N_4O_8$: 1095.16 found: 1095.17. Anal. Calcd. For $C_{72}H_{46}N_4O_8$: C 78.96 H 4.23, N 5.12 %; found: C 78.72, H 4.22, N 5.20 %. FTR-IR cm^{-1}: 3319 (ν_{NH} porphyrin), 2964–2861 (ν_{CH} porphyrin), 1735 ($\nu_{C=O}$ ester), 1267 (ν_{C-O} ester), 969 (δ_{CCH} porphyrin).

Synthesis of the (meso-tetrakis[4 (benzoyloxy)phenyl] porphyrinato)magnesuim(II) complex [Mg(TPBP)]: H_2TPBP (0.6 g, 0.54 mmol) was dissolved in DMF (150 mL). The solution was heated under reflux with magnetic stirring. Upon dissolution of the H_2TPBP, $MgCl_2$ (1 g, 10.8 mmol) was added. The reaction mixture was stirred for 6 hours. thin-layer chromatography (alumina, using CH_2Cl_2 as eluant) indicated no free base porphyrins at this point. After that, the solution was cooled to 50-60 °C and H_2O (50 mL) was added into it. Obtained solid was filtrated and washed with hexane. The resulting was vacuum-dried to afford 66 % yield of MgTPBP. ^{1}H NMR (300 MHz, $CDCl_3$) δ(ppm) 8.96 (s, 8H, Hβ-pyrrol), 8.67 (d, 8H, *J*=6.4 Hz), 8.36 (d, 8H, *J*=8.33 Hz), 7.2 (d, 8H, *J*=8.8 Hz), 7.62 (m, 12H). UV/vis [λ_{max} (nm) in CH_2Cl_2, (log ε)]: 427 (5.86), 565 (4.42), 605 (4.16). MS [ESI]: m/z calcd for

$C_{72}H_{44}MgN_4O_8$: 1117, 3082, found: 1117, 3848. Anal. Calcd. For $C_{72}H_{44}N_4O_8$: C 77.39 H 3.97, N 5.01 %; found: C 75.22, H 3.22, N 5.20 %. FTR-IR cm^{-1}: 2926 (ν_{CH} porphyrin), 1757 ($\nu_{C=O}$ ester), 1267 (ν_{C-O} ester), 1030 (δ_{CCH} porphyrin).

Synthesis and crystallization of [Mg^{II}(TPBP)(HTMA)$_2$] (1): MgTPBP (20 mg, 0.017 mmol) was mixed with the bidentate ligand hexamethylenetetramine (HTMA) (90 mg, 0.80 mmol) in 5 mL of DCM solvent. The mixture was stirred at room temperature for 3 hours. Crystals of the desired complex were obtained by slow diffusion of n-hexane through the dichloromethane solution. ^{1}H NMR (300 MHz, $CDCl_3$) δ(ppm) 9.01 (s, 8H, Hβ-pyrrol), 8.42 (d, 8H, *J*=8.4 Hz), 8.30 (d, 8H, *J*=8.7 Hz), 7.73 (d, 8H, *J*=8.2 Hz), 7.64 (m, 16H), 3.03 (s, H-ligand). UV/vis [λ_{max} (nm) in CH_2Cl_2, (log ε)]: 435 (5.88), 576 (4.33), 617 (4.40), 591 (5). MS [ESI]: m/z calcd for $C_{78}H_{56}MgN_8O_8$: 1257.63, found: 1258, 38. Anal. Calcd. For $C_{84}H_{68}MgN_{12}O_8$.C; 72.17; H; 4.89; N; 12.02. Found: C; 68.19; H; 4.79; N; 12.02. FTR-IR cm^{-1}: 2924-2863 (ν_{CH} porphyrin), 1740 ($\nu_{C=O}$ ester), 1267 (ν_{C-O} ester), 1241 (ν_{C-N} ligand), 1018 (δ_{CCH} porphyrin), 994 (δ_{NCH} ligand).

Synthesis and crystallization of [Mg^{II}(TPBP)(DABCO)$_2$] (2): [Mg(TPBP)] (20 mg, 0.017 mmol) and DABCO (90 mg, 0.80 mmol) in 5 mL of DCM were stirred of 3 hours at room temperature. The colour of the reaction mixture changed from purple to green-blue. Crystals of [Mg^{II}(TPBP)(DABCO)$_2$] (**2**) were prepared by slow diffusion of hexanes into the dichlorometane solution. ^{1}H NMR (300 MHz, $CDCl_3$) δ(ppm) 9.00 (s, 8H, Hβ-pyrrol), 8.45 (d, 8H, *J*=8.2 Hz), 8.30 (d, 8H, *J*=8.7 Hz), 7.75 (t, 4H, *J*=8.8 Hz), 7.67 (m, 16H), 7.30 (s, 12H). UV/vis [λ_{max} (nm) in CH_2Cl_2, (log ε)]: 429 (5.88), 565 (4.44), 605 (4.20). MS [ESI]: m/z calcd for $C_{78}H_{56}MgN_6O_8$: 1228.40 found: 1229.40. Anal. Calcd. for $C_{84}H_{68}MgN_8O_8$.C; 75.19; H; 5.10; N; 8.35. Found: C; 72.82; H; 5.00; N; 7.91. FTR-IR cm^{-1}: 3032 (ν_{CH} DABCO), 2930-2856 (ν_{CH} porphyrin), 1736 ($\nu_{C=O}$ ester), 1058 (δ_{CCH} porphyrin), 700 (δ_{NCH} ligand).

2.2. X-ray diffraction study

Crystals of (**1**) and (**2**) complexes suitable for single crystal X-ray diffraction were obtained by the method described below: Purple-Blue crystals with 0.22 mm x 0.14 mm x 0.25 mm approximate dimensions were selected for the X-ray diffraction experiment. Data collections for (**1**) and (**2**) were performed on a Bruker APEX-II diffractometer and a Bruker D8 venture diffractometer, respectively. All diffractometers were equipped with graphite monochromated Mo Kα radiation (λ = 0.71073 Å) and intensity data for all compounds were collected by the narrow frame method at room temperature. All structures were solved by

direct method using SIR-2004 [38] and refined by full-matrix least-squares on F_2 using the SHELXL-97 program [39]. Data were corrected for absorption effects by the Multi-Scan method [40].

2.3. Spectroscopy and photophysical measurements

Absorption spectral measurements were carried out using a Varian Cary 5000 spectrophotometer. ^{1}H NMR spectra were recorded on a Bruker Avance 300 MHz spectrometer. Infrared spectra were measured on a Nicolet Impact 410 spectrophotometer and the Thermo Scientific "Q Exactive" mass spectrometer was operated under electrospray ionization (ESI) in positive mode. The elemental analyses were recorded on a Flash EA 1112 Series Thermo Electron fitted with a Porapak column PTFE + MX5 microbalance Mettler Toledo. Fluorescence spectra and quantum yield measurements were performed using a Varian Cary Eclipse luminescence spectrofluorimeter.

2.4. Antibacterial screening

Pathogenic strains were cultured on nutrient agar at 37 °C for 24h. Then, pure colonies were suspended in 10 ml of physiological medium, mixed well for 5 min and suspensions were adjusted to 0.5 McFarland standard turbidity. One milliliter of bacterial suspension was spread over Muller Hinton Agar medium plates and incubated for 30 min at 37 °C. After that, 6 mm diameters wells were dug in agar medium using sterile glassy borer. The Mg(II) complexes were prepared in DMSO (1 mg/mL) and introduced into the respective wells, one of the wells was supplemented with DMSO as control. These plates were placed in a 37 °C incubator for 24h to allow bacterial growth. After 24h, the diameters of the clear zone of inhibition surrounding the sample were measured in millimeters by digital caliper.

2.5. Computational details

3D Hirshfeld surfaces and associated 2D fingerprint plots were performed using the CrystalExplorer 3.1 software [30] and TONTO [33-34] system. In order to explain the activity and the semi-conductive behaviour of our compounds, we modelled the energy gap from HOMO to LUMO using Gaussian 09W [41] and GaussView 5.0.8 [42] programs. The DFT approach and effective core potentials (ECPs) (LANL2DZ basis and ECP built-in) have been utilised in order to representing the metal. The B3LYP method with 6-31+G(d,p) basis set was used for all atoms except for the magnesium [43-44]. The electron- density distribution of HOMO and LUMO is plotted and visualising using GaussView.

3. Results and discussion

3.1. Crystal structure description of (1) and (2)

Crystallographic data and structural refinement details of (**1**) and (**2**) are shown in Table 1. Complex (**1**) crystallizes in the monoclinic system with P 2_1/n space group. The unit cell parameters are: a = 17.391(1) Å, b = 11.559(7) Å, c = 19.408(1) Å; β = 113.2 (2)°; Z = 2. The complex (**2**) crystallizes in the triclinic system with P -1 space group; a = 10.278(5) Å, b = 10.443(5) Å, c = 16.360(5) Å, α = 81.87(5)°, β = 83.6(5)°, γ = 78.041(5)°, Z = 2. Selected bond lengths and angles for both complexes are listed in Table S1.

Table 1. Crystal data and structure refinement of (**1**) and (**2**) complexes.

	Complex (**1**)	Complex (**2**)
Chemical formula	C_{84} H_{68} Mg N_{12} O_8	C_{84} H_{68} Mg N_8 O_8
Formula weight	1397.81	1341.77
Crystal system	monoclinic	triclinic
Space group	P 2_1/n	P$\bar{1}$
a [Å]	17.3912(9)	10.278(5)
b [Å]	11.5588(7)	10.443(5)
c [Å]	19.4079(11)	16.360(5)
α[Å]	90	81.867(5)
β [Å]	113.230(2)	83.561(5)
θ [Å]	90	78.041(5)
V [Å^3]	3585.1(4)	1694.4(13)
Z	2	2
*D*calcd. [g/cm^3]	1.295	1.315
μ [mm^{-1}]	0.093	0.769
Max./min. transmission	0.809 / 0.996	0.857 / 0.898
F(000)	732	704
Crystal size [mm]	0.45 / 0.16 / 0.04	0.2 / 0.18 / 0.14
T (K)	150	100
Unique data	8053	6891
Unique obsd data	3954	5967
Final *R* indices	R_1 = 0.0761,	R_1 = 0.0424,
	wR_2 = 0.2291	wR_2 = 0.1030

The asymmetric units of both complexes present one half [Mg(TPBP)(L)] (L = HTMA or DBCO) complex. The coordination geometry around the Mg(II) cation in (**1**) and (**2**) is octahedral (Fig.s 1 and 2), where the four donor N atoms of pyrrole rings of the TPBP porphyrin occupy the equatorial positions. The donor N atoms of axial ligands, the HTMA (for **1**) and of the DABCO (for **2**), occupy the apical positions.

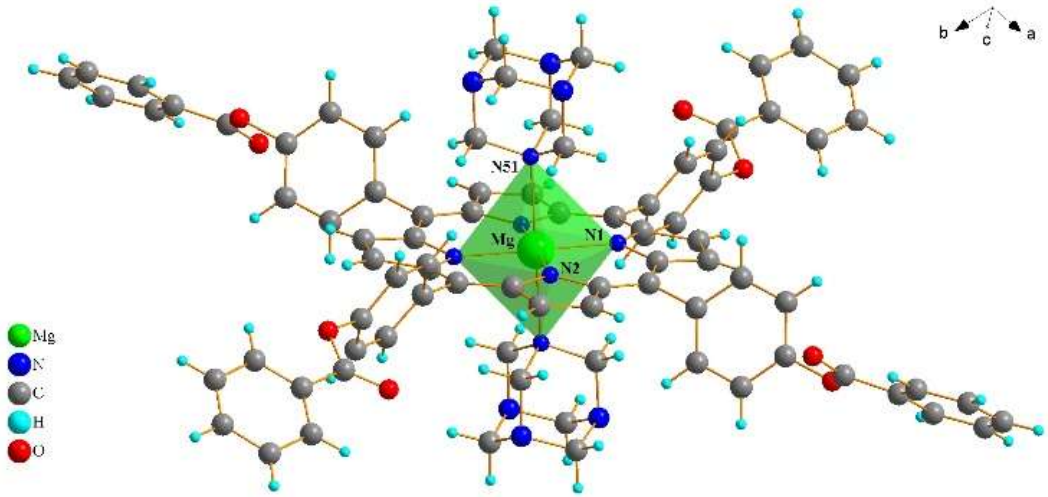

Fig. 1. Molecular structure of (**1**). (2-column figure)**.**

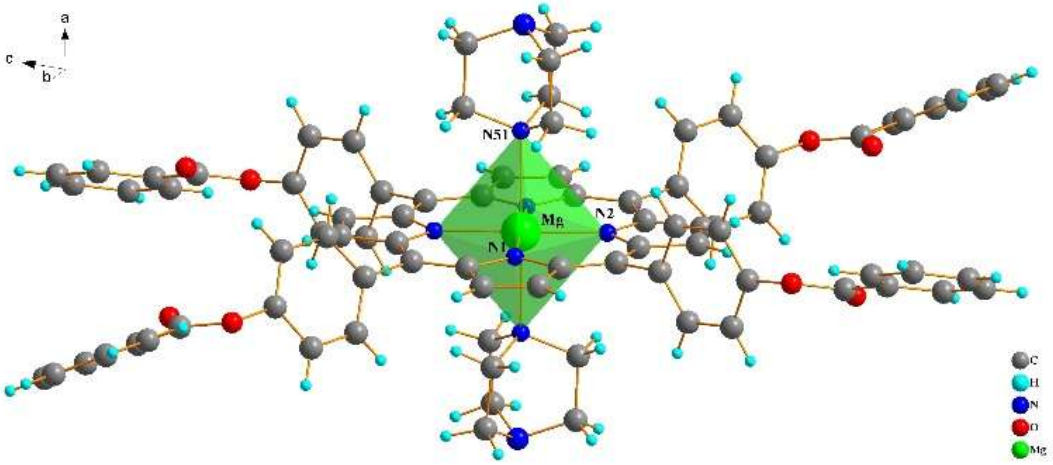

Fig. 2. Molecular structure of (2). (2-column figure).

As can be seen from Table S2, Mg-Nax distances range between 2.438 and 2.437 Å indicate the strong coordination of two ligands HTMA and DABCO to metalloporphyrin which seems in agreement with Mg—Nax bond length (2.473 Å) observed in previously studied similar complex [Mg(TPP)·$(HTMA)_2$] [45]. For [Mg(TPP)$(4\text{-pic})_2$] and [Mg(OEP)$(py)_2$], the Mg—Nax bonds are 2.386 and 2.389 Å, respectively [46,47], which seem to be little shorter than those in title complexes. However, the Mg—Nax distance for [Mg(tn-OEP)$(4,4'\text{-bpy})_2$] is found to be shorter with 2.259 and 2.272 Å values [48]. In comparison with their analogues of the complexes, The Mg—Nax (HTMA) distance is shorter than those of six-coordinated (HTMH)-zinc porphyrins [49]. For the DABCO magnesium porphyrin derivative (**2**) the Mg—N(DABCO) distance is very close to the related DABCO-Cobalt porphyrin (Co—N(DABCO = 2.457 Å), but very shorter than those of related manganese porphyrin [50]. The four Mg—Np bonds consist of two sets of equal length 2.074

and 2.066 Å as exists in the opposite pairs and fall on the range [2.063 – 2.100 Å] of other reported Mg(II)-porphyrins (Table S2).

Additional quantitative information of two structures are given in Fig. 3, which displays the detailed displacements of each porphyrin core atom (in units of 0.01 Å) from the 24-atom mean planes. The top panels show that porphyrin cores of [Mg^{II}(TPBP)$(HTMA)_2$] (**1**) and [Mg^{II}(TPBP)$(DABCO)_2$] (**2**) have a near-planar porphyrin macrocycle conformation. The displacement of *meso* and beta-carbons from the least-squares plane of $C_{20}N_4$ pophyrinato core are ± 0,033 and ± 0,027 Å respectively, these displacements are very close to those found in analogous compounds [48].

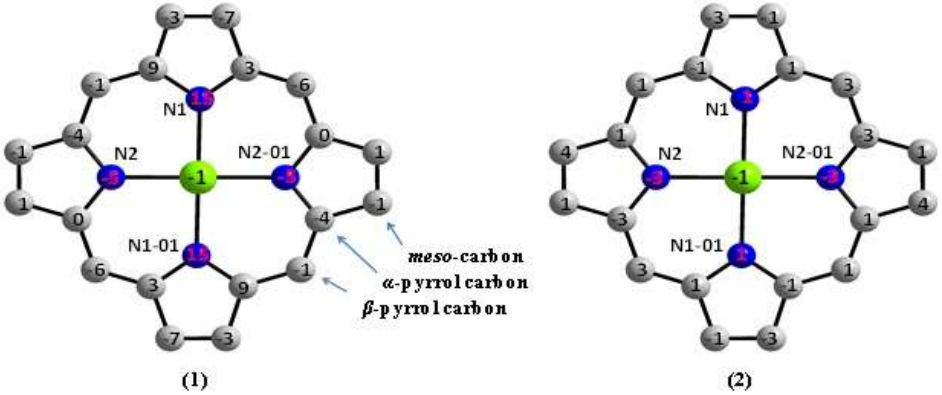

Fig. 3. A formal diagrams of complexes (**1**) and (**2**) core showing the perpendicular displacement of each atom, in units of 0.01 Å, from the mean plane of the 24-atom core. (2-column figure).

The supramolecular assemblies for both complexes are shown in Fig. 4 and 5. The stability and cohesion of crystal packing for complex (**1**) are assured by intramolecular C54–H54···N2 hydrogen bond, and by weak C–H···Cg π interactions involving carbon atoms (C53 and C54) from hexamethylenetetramine coordinated and the centroids of the pyrrole of the *meso*-porphyrin. On the other hand, neighboring molecules are linked one to the other by intermolecular C–H···O and C–H···N hydrogen bonds, and by weak C45–H45···Cg8 π interaction involving a carbon atom (C45) of phenyl ester and the centroid of the same function of neighbouring molecule (C···Cg distance range 3.710 Å) (table 2).

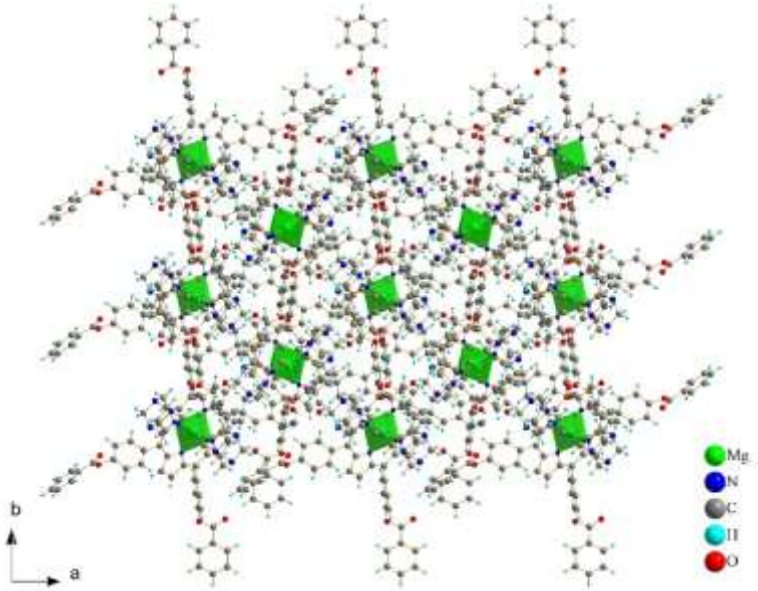

Fig. 4. Supramolecular atomic arrangement along the *c*-axis of (**1**). (2-column figure)

Similarly, molecular structure and crystal packing for complex (**2**) are stabilised by inter-and intramolecular C–H···O hydrogen bonds, and by weak C–H···Cg π interactions involving several centroids (Cg) of the pyrrole and *meso*-porphyrin phenyl groups such as the C–H···O interactions which range between 3.447(2) and 2.732(2) Å and the C–H···Cg π interactions which vary between 3.521(2) and 3.823(2) Å (Table 2).

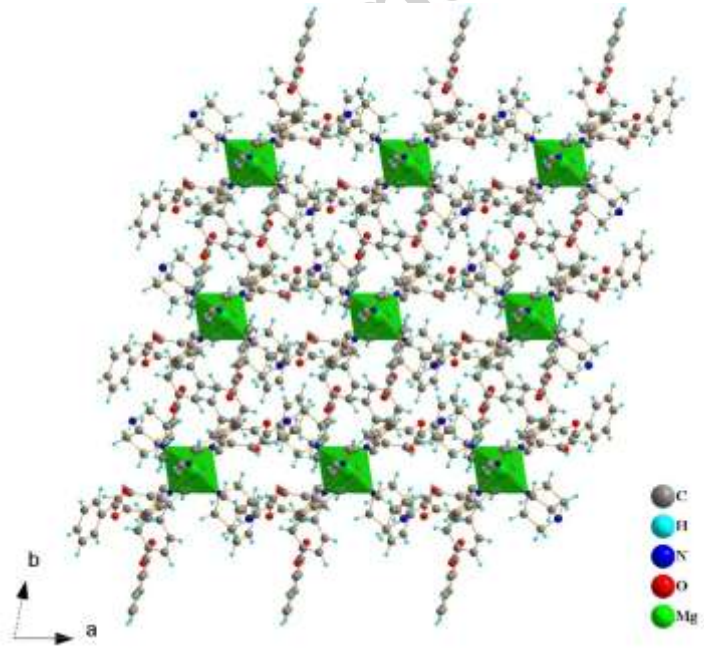

Fig. 5. Supramolecular atomic arrangement of along the *c*-axis of (**2**). (2-column figure).

Table 2. Inter-and intramolecular interactions for (**1**) and (**2**).

D-H …A [a]	Symmetry of A	D-H…A	D…A
Complex 1			
C15-H15…O39	1/2+x,3/2-y,-1/2+z	148	3.429(6)
C24-H24…O19	3/2-x,1/2+y,-1/2-z	152	3.280(2)
C32-H32…O19	1-x,2-y,-z	136	3.250(5)
C42-H42…N59	-1+x,y,z	146	3.437(6)
C54-H54A…N2	-1+x,y,z	113	3.152(5)
C45-H45…Cg8	1/2-x,-1/2+y,-1/2-z	158	3.710(7)
C53-H53A…Cg1	1-x,1-y,-z	109	3.352(5)
C53-H53B…Cg1	1-x,1-y,-z	104	3.352(5)
C54-H54A…Cg2	x,y,z	136	3.608(4)
Complex 2			
C15-H15…O39	1-x,-y,-z	152	3.447(2)
C45-H45…O37	1-x,-y,-z	100	2.732(2)
C22-H22…Cg6	2-x,1-y,-z	158	3.823(2)
C35-H35…Cg7	1-x,-y,-z	163	3.521(2)
C53-H53A…Cg2	x,y,z	123	3.559(2)
C55-H55A…Cg8	1-x,-1-y,1-z	157	3.782(2)

[a] *D = donor atom and A = acceptor atom.*
*Complex (**1**): Cg1 is the centroid of the N1-C1-C2-C3-C4 five membered ring, Cg2 is the centroid of the N2-C6-C7-C8-C9 five membered ring, Cg8 is the centroid of the C20-C21-C22-C23-C24-C25 six membered ring. Complex (**2**): Cg1 is the centroid of the N1-C6-C7-C8-C9 five membered ring, Cg6 is the centroid of the C11-C12-C13-C14-C15-C16 six membered ring, Cg7 is the centroid of the C20-C21-C22-C23-C24-C25 six membered ring, Cg8 is the centroid of the C31-C32-C33-C34-C35-C36 six membered ring.*

3.2. Hirshfeld surfaces analysis

Intermolecular interactions are receiving extensive attention in the area of crystal engineering owing to their potential role in preparation of novel compounds of desirable properties. They can be characterised by X- ray diffraction technique likewise in the light of several computational methods. In this work, Hirshfeld surface analysis was performed to more understand and identify individual types of non-covalent intermolecular contacts and their contribution on crystal packing.

The 3D Hirshfeld surfaces [21-24] and 2D fingerprint plots [31-32] of our complexes are illustrated in Fig. S1 and S2, which showing surfaces that have been mapped with d_{norm}, shape index and curvedness. The generated surfaces for both structures have almost similar shapes. The d_{norm} surfaces were mapped over a fixed colour scale of -0.241 (red) to 2.001 (blue) for (**1**) and -0.247 (red) to 1.706 (blue) for (**2**).

Mainly two categories of non-covalent intermolecular interactions are presented in both (**1**) and (**2**) crystal structures: isotropic or directional (C···C, C···H, H···H …) and anisotropic or non- directional (especially C–H···O and C–H···N hydrogen bonds).

Fig. 6 report a Molecular Hirshfeld surface mapped with d_{norm}, showing the C–H···O intermolecular hydrogen bonds in the crystal packing of (**1**). The surface is drawn as transparent to show the molecular moieties. Here we provide a discussion only for complex (**1**), just as an example to better explain the principle of our analysis (complete information is provided in Fig. S1 and S2 given as supplementary material).

As indicated in equation 1, The d_{norm} property is a sum of two quantities, d_i and d_e. which are normalised by the van der Waals radius of the atom involved. d_i is the closest internal distance from a given point on the surface and d_e is the closest external contact.

$$\boldsymbol{d_{norm}} = \frac{\boldsymbol{d_i - r_i^{vdw}}}{\boldsymbol{r_i^{vdw}}} + \frac{\boldsymbol{d_e - r_e^{vdw}}}{\boldsymbol{r_e^{vdw}}} \qquad \text{(Eq. 1)}$$

In the colour scale, negative values of d_{norm} are visualized by the red colour, indicating contacts shorter than the sum of Van Der Waals radii. The white colour designates intermolecular distances close to vdW contacts with d_{norm} equal to zero. However, contacts longer than the sum of r^{vdw} with positive d_{norm} values are indicated in blue. As seen on the Hirshfeld surface, H···O contacts (C15-H15…O39 and C24-H24…O19) are observed as intense red spot. This shows that its distances are significantly shorter than the corresponding sum of vdW radii, indicating its important role in crystal packing.

The 2D fingerprint (d_i versus d_e) plots, illustrated in Fig. S1 and S2, highlight a particular atom pair close contacts. This decomposition enables the separation of contributions from different non-covalent interaction types which overlap in the full fingerprint. Fig. 7 summarise the distribution of individual intermolecular interactions on the basis of fingerprint maps of (**1**) and (**2**). For both complexes, crystal structures are dominated by H···H and C···H contacts, comprising respectively 55.6 and 27.1 % for (**1**) and 53.6 and 25.3 % for (**2**). The H···O intermolecular interactions appear as two spikes pointing toward the lower left of the plot (Fig. S1 and S2) . The proportion of H···O contacts comprises 14% and 12.3% of the total surface, respectively, for (**1**) and (**2**).

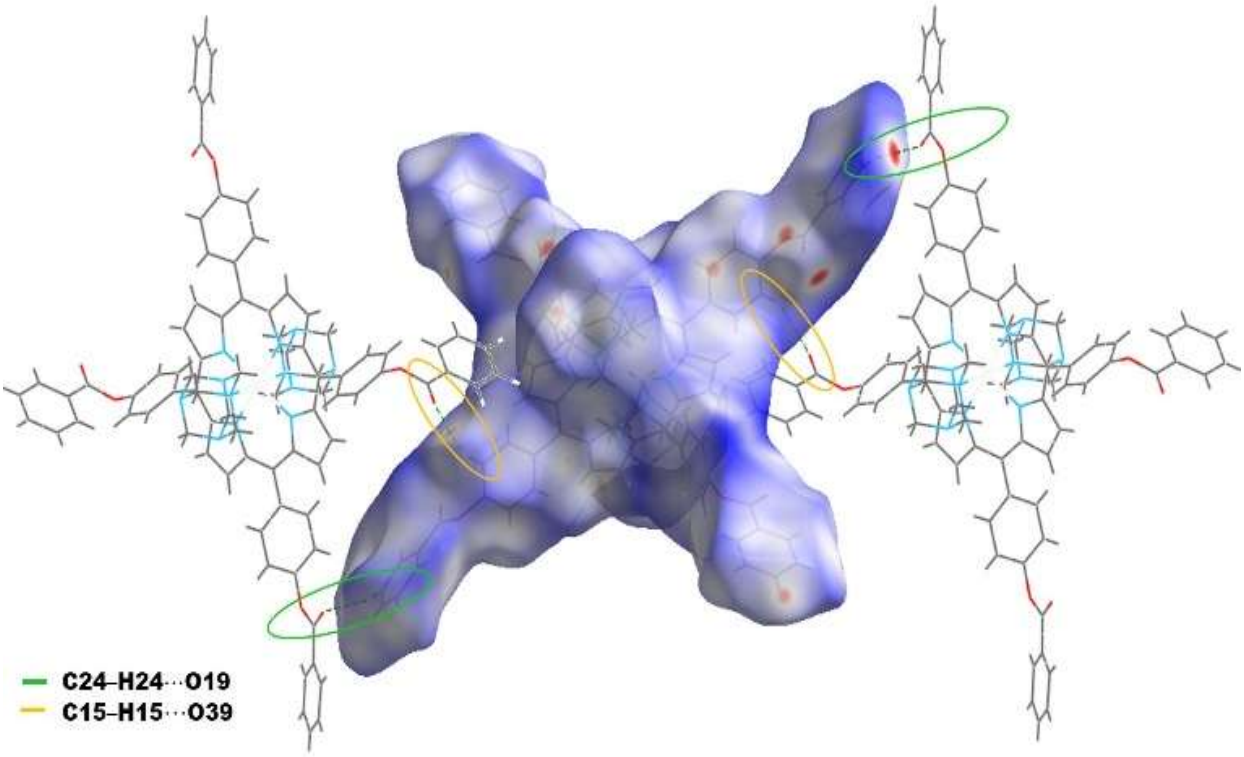

Fig. 6. Molecular Hirshfeld surface mapped with d_{norm} about a reference molecule , highlighting the C–H···O intermolecular hydrogen bonds in the crystal packing of (**1**). (single-column figure)

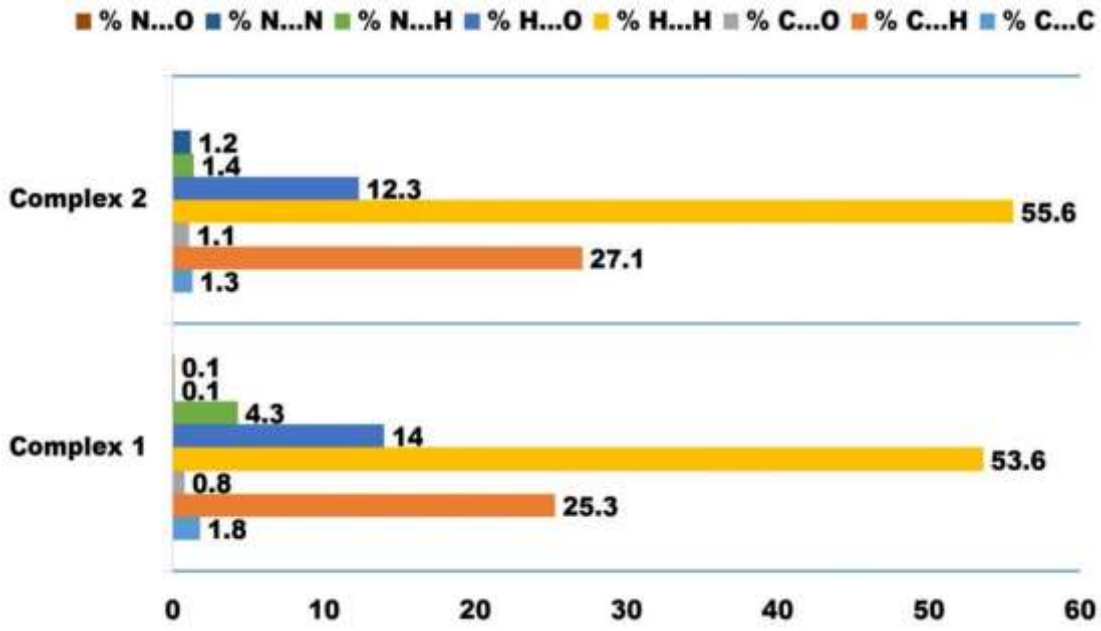

Fig. 7. Distribution of individual intermolecular interactions on the basis of Hirshfeld surface of (1) and (2). (single-column figure)

In addition and by comparing the sky blue and grey colour in Fig. 7, it is seen that the relative contribution of C···C and C···O contacts are comparable for both complexes. However, the fourth main contribution ,arises from N···H contacts, comprises two slightly different proportions of 4.3 % for (**1**) and 1.4 %for (**2**). Moreover, The structures are also described by N···N and N···O contacts, even with negligible contributions

From generated Hirshfeld surfaces, the globularity (*G)* [25] and asphericity [26-27] (*Ω)* quantitative measures were also performed in order to determine the molecular surface nature and the anisotropy of studied molecules. The globularity concept gives the degree to which the surface area varies in value for a sphere of the same volume. It is expressed as following:

$$\boldsymbol{G} = \frac{\boldsymbol{S}_{\boldsymbol{sphere}}}{\boldsymbol{S}_{\boldsymbol{H}}} = \frac{(36\pi)^{1/3}\, \boldsymbol{V}_{\boldsymbol{H}}^{2/3}}{\boldsymbol{S}_{\boldsymbol{H}}} \qquad \text{(Eq. 2)}$$

where $\boldsymbol{S}_{\boldsymbol{H}}$ (1272,82 Å^2 for(**1**), 1282,47 Å^2 for (**2**)) and $\boldsymbol{V}_{\boldsymbol{H}}$ (1772,21 Å^3 for(**1**), 1741,12 Å^3 for (**2**)) are the surface area and volume of the Hirshfeld surfaces respectively.

Asphericity is a measure of the anisotropy of an object. Each point of the surface is treated as an object. when applied on the atomic positions, (*Ω)* is defined by the equation:

$$\boldsymbol{\Omega} = \frac{1}{2}\left\{\sum_{i<j}\left(\boldsymbol{\lambda}_i - \boldsymbol{\lambda}_j\right)^2\right\}\left\{\sum_i (\boldsymbol{\lambda}_i)^{-2}\right\} \qquad \text{(Eq. 3)}$$

where $\boldsymbol{\lambda}_{\boldsymbol{i}}$ are the principle moments of inertia of the molecule.

Computed values of globularity are 0,556 and 0,546 for (**1**) and (**2**) respectively which demonstrating that both molecular surfaces are more structured as they differ to a sphere (< 1). The asphericity is found to be 0,146 for (**1**) and 0,179 for (**2**).

In order to elucidate the packing arrangement modes and provide some chemical insight through the manner in which molecules contact with its surrounding crystalline environment, Shape Index and Curvedness surfaces properties have been also generated [28-29] (Fig. 8). The shape index S and curvedness C are defined as following (Eq. 3 and 4):

$$\boldsymbol{S} = \frac{-2}{\pi}\boldsymbol{arctan}\frac{K_1+K_2}{K_1-K_2}$$ (Eq. 4) and $$\boldsymbol{C} = \frac{2}{\pi}\boldsymbol{ln}\sqrt{\frac{K_1^2+K_2^1}{2}}$$ (Eq. 5)

Where κ_1 and κ_2 are principal curvatures calculated at a point on the surface.

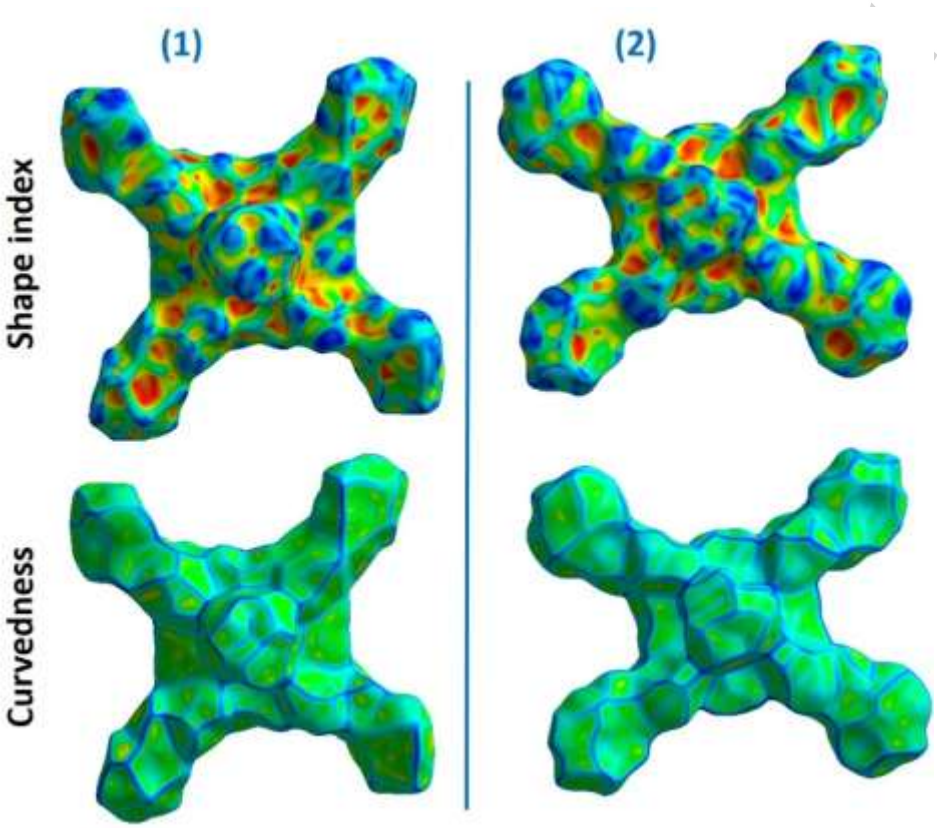

Fig. 8. Shape index and Curvedness surfaces for (**1**) and (**2**) molecules. (2-column figure)

For both complexes, the red circles and triangles appeared in the Shape Index as concave regions indicate hydrogen acceptor centres, while blue convex regions designate the H donor atoms. The relatively large green regions, observed as flat patches in the curvedness mapped surfaces, indicate the presence of C–H···Cg π interactions between molecules (Fig. 8).

3.3. IR spectroscopy

FT-IR spectra were recorded and examined for both complexes (Fig. S3 and Fig. S4). Since (**1**) and (**2**) have almost the same functional and skeletal groups (CH, C=O, C–O, CCH, CNH…), the assignment of its vibration modes are relatively easy because they were observed at very similar wavenumber in both complexes The bands located at 2964-2863 cm^{-1} and 2856-3032 cm^{-1} domains are respectively assigned to CH stretching mode for complex (**1)** and (**2)**. The *ν*(C=O) ester group band are observed at 1740 cm^{-1} for (**1)** and 1736 cm^{-1} for (**2**). The *δ*(CCH) bands appeared at 1018 and 1058 cm^{-1}. The IR spectra confirm the presence of the axial ligands. The IR spectrum of the HTMA-magnesium derivative (**1**) shows two characteristic bands at 994 cm^{-1} *δ*(NCH) and 1241 cm^{-1} ν(CN) which attributed to the coordinated HTMA ligand (Fig. S3). For the DABCO-magnesium derivative (**2**) the IR spectrum exhibits band at 3032 cm^{-1} attributed to *ν*(CH) of the methylene group (Fig. S4).

3.4. Photophysical properties

The absorption spectra of the H_2TPBP and [Mg(TPBP)] starting materials, as well as those of complexes (**1**) and (**2**), are illustrated in Fig. 9. The free base *meso*-porphyrin H_2TPBP shows the λ_{max} values of the *Soret* band at 419 nm and *Q* bands at 515, 551, 590 and 646 nm. The [Mg(TPBP)], exhibit electronic spectra, which are slightly red shifted compared to those of the free base, with *Soret* bands at ca. 427 nm and *Q*(1,0) and *Q*(0,0) bands at ca. 565 and 605 nm respectively. On the other hand, the neuters complexes spectra [Mg(TPBP)(L)] (L = HTMA or DABCO) exhibit larger redshifts of the Soret and Q bands (up to 11 nm for (**1**) and 5 nm for (**2**)) than those of the anionic complexes of the type [Mg(TPP)(X)], in which X is a pseudohalide (N_3^-, NCO^-, NCS^-, NCO^-) [51-52] ligand (Table S3).

The optical band gap (Eg-op), which corresponds to the energy difference between the levels of the HOMO and LUMO, is obtained from the UV-visible spectra. This energy is calculated from the value of the tangent to the *Q*(0,0) absorption band (λ_{gap}). The Eg-op values are 2.002 eV for (**1**) and 2.041 for (**2**), which are in the normal range of magnesium porphyrin complexes [53].

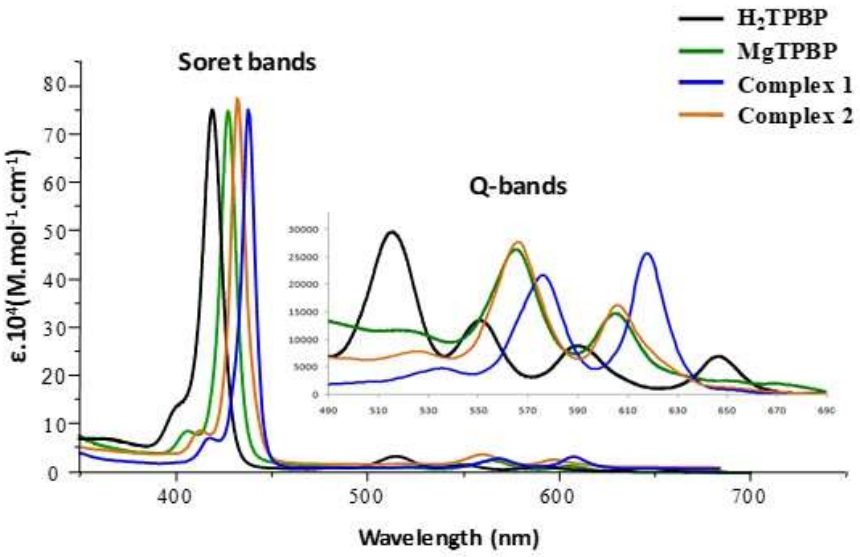

Fig. 9. UV/Vis absorption spectra of H_2TPBP, [Mg(TPBP)], [Mg^{II}(TPBP)(HTMA)$_2$] (**1**) and [Mg^{II}(TPBP)(DABCO)$_2$] (**2**) in CH_2Cl_2 solution at concentrations of ca. 10^{-6} M. (2-column figure)

The emission and excitation spectra of the free porphyrin, metalloporphyrin and complexes (**1**) and (**2**) are shown in Fig. S5. The emission spectra data and the fluorescence quantum yields (Φ_f) of these complexes are given in Table S4. Excitation of the *Soret* band of H_2TPBP porphyrin (Fig. S5a) results in two emission bands S2 →S0 centered at 652 nm (S2 [*Q*(0,0)] →S0) and 719 nm (S2 [*Q*(0,1)] →S0). In the case of metalloporphyrin [Mg(TPBP)] (Fig. S5b), excitation of the *Soret* bands results in two emission bands S2→S0 centered at 611 (S2 [*Q* (0.0)] →S0) and at 665 nm (S2 [*Q* (0,1)] →S0). Compared with the fluorescent bands at 652 and 719 nm of TPBP, the emission peaks of porphyrin ligand were red-shifted by 41 nm.

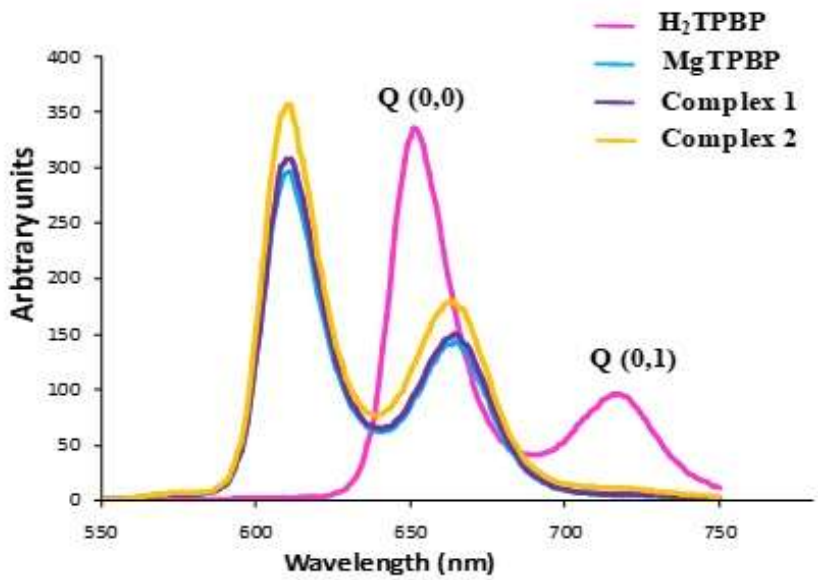

Fig. 10. Emission spectrum of the starting material H_2TPBP, [Mg(TPBP)], complex (**1**) and complex (**2**). (2-column figure)

The fluorescence bands of the complexes (**1**) and (**2**) were between 611 and 666 nm, which are in the same range as MgTPBP (611 and 665 nm) (Fig. 10). However, the λ_{max} values of the *Q*(0,0) and *Q*(0,1) bands of (**1**) and (**2**) are close to those of the related Mg porphyrin derivatives (Table S4). The fluorescence quantum yields of H_2TPBP, (**1**) and (**2**) are in the range of [0.050 - 0.065] which are close to the related magnesium metalloporphyrins.

3.5. Frontier molecular orbital analysis

In the present work, we modelled and highlight the contour surfaces of the frontier molecular orbitals for both complexes (**1**) and (**2**) using the DFT approach with B3LYP/ 6-31+G(d,p) and LANL2DZ basis sets. The LUMO and HOMO orbitals represent the ability to obtain or to donate an electron, respectively. HOMO-LUMO energy gap, was used to provide insights into the stability and chemical reactivity of molecules. A molecule with a small frontier orbital gap termed as soft molecule is more polarizable and is generally associated with a high chemical reactivity and a low kinetic stability [54-57]. Furthermore, compounds with smaller band gaps (<3eV) behave as semiconductors [57]. As shown in Fig. 11, the HOMO and LUMO electron density are mainly distributed on the pyrrole rings and phenyl atoms of the(H_2TPBP) porphyrin groups. The computed energy gap (E_{LUMO}-E_{HOMO}) values are found to be 1.86648 and 1.90973 eV, respectively for (**1**) and (**2**), Which seem to be in good agreement with corresponding experimental values obtained from UV-visible spectra. Consequently, these relatively large HOMO-LUMO gap means high excitation energies for many of the excited states, a good stability and a high chemical hardness for our studied complexes. This also reveals that both (**1**) and (**2**) can be classified as semiconductors [59-61].

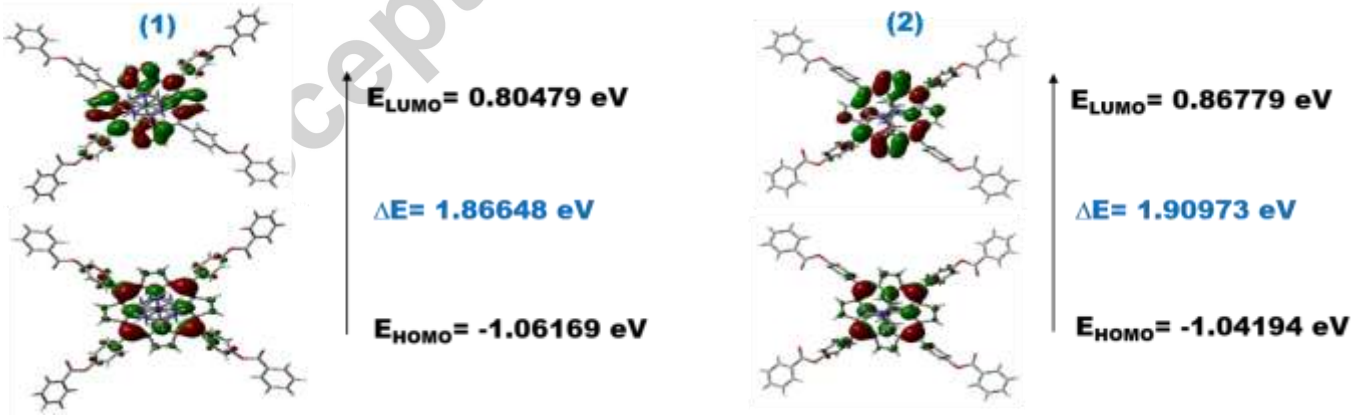

Fig. 11. Frontier molecular orbitals (HOMO and LUMO) plots of (1) and (2). Contour surfaces of orbital amplitude 0.02 (red) and −0.02 (green) are shown. (single-column figure)

3.6. Antibacterial activity tests

A variety of biological activities exhibited by porphyrins are due to the fact that natural and synthetic porphyrins have relatively low toxicity in vitro and in vivo and they possess antitumor [62-63] and antioxidant effects [64]. In the present work, the in vitro antibacterial activity of the free porphyrin base H_2TPBP, Mg(TPBP), [Mg^{II}(TPBP)(HTMA)$_2$] (**1**) and [Mg^{II}(TPBP)(DABCO)$_2$] (**2**) against two Gram-positive bacteria (*Staphylococcus aureus* (ATCC 25923) and *Enterococcus faecalis* (ATCC 29212)) and two Gram-negative bacteria (*Pseudomonas aeruginosa* (ATCC 27853) and *Escherichia coli* (ATCC 35218)) was assessed using well agar diffusion assay as described by Abdelkarim Mahdhi et al (2012) [65]. *In vitro* antibacterial activity of synthesised compounds was evaluated against certain pathogenic bacteria and compared by standard drug tetracycline [66]. The diameters of inhibition zones observed with the well diffusion method are shown in Fig. 12. Based on zones of inhibition results, the lowest activity is observed for the free porphyrin base H_2TPBP. Contrariwise, the Mg(TPBP), starting material and the complexes **1** and **2** show better anti-bacterial activity against the three strains (*P. aeruginosa*, *E. faecalis* and *E. coli*). These values are higher than the standard drug tetracycline [66]. these magnesium derivatives show 20 mm, 18 mm and 12 mm in diameter of zone inhibition against *P. aeruginosa* and 13 mm, 13 mm and 16 mm in diameter of zone inhibition against *E. faecalis*. They also produced 18 mm, 17 mm and 15 mm in diameter of zone inhibition against *E. coli*. Tetracycline shows ~12 mm in diameter of zone inhibition against *P. aeruginosa* and *E. coli* [66]. In comparison with their analogues, our studied complexes possess diameters of zones of inhibition higher than these obtained with *meso*-tetrakis(40-trifluoromethylphenyl) porphyrin metallated by Ni (II), Cu (II), and Zn (II), especially on the microbial strain *E. coli* (between 15 and 19 mm) [67]. However, they are less active than the Co(III) porphyrins (*S. Aureus* ~ 24 mm) [68].

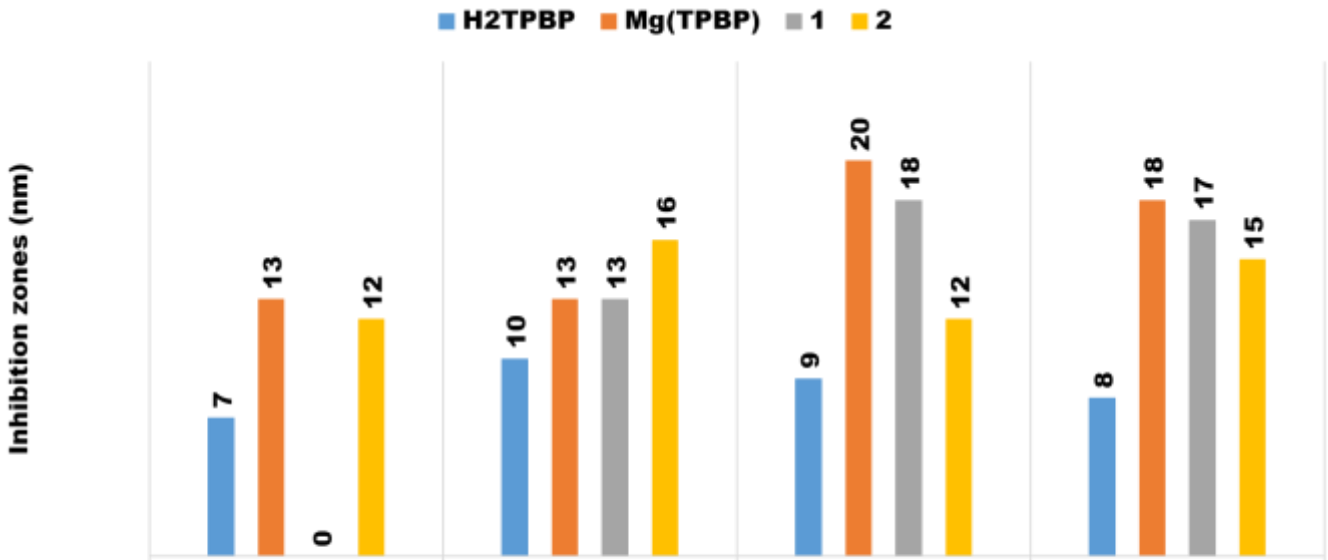

	S. aureus	E. faecalis	P. aeruginosa	E. coli
H2TPBP	7	10	9	8
Mg(TPBP)	13	13	20	18
1	0	13	18	17
2	12	16	12	15

Fig. 12. in *vitro* antimicrobial activity of (**1**) and (**2**). (single-column figure)

4. Conclusions

In the present work, we have synthesised, two novel six-coordinate magnesium porphyrin complexes. This is significant since the starting material, *meso*-porphyrin: tetrakis[4-(benzoyloxy)phenyl]porphyrin (H_2TPBP) was prepared for the first time. The most important conclusions, obtained in this work, can be summarized as follows: the coordination geometry of Mg(II) cations is octahedral; the supramolecular assemblies are assured by both hydrogen bonding and weak C–H···Cg π interactions; Despite the differences observed in energy gap values, the general agreement between experimental and computational results is good; antibacterial activities of both complexes were evaluated and confirmed. As Metal–organic frameworks (MOFs) and due to its size, shape, crystal packing nature, and its organic ligand functional groups, prepared complexes can have many practical uses such as gas storage and catalysis.

Conflicts of interest

The authors confirm that "there are no conflicts of interest to declare"

Electronic supplementary information (ESI)

Electronic Supplementary Information (ESI) available: Main chemical preparation steps (scheme). Crystal data, Structure refinement and Geometric parameters for both complexes. UV-Vis, Fluorescence and IR spectra Data. Hirshfeld surfaces and fingerprint plots. Crystallographic data: CCDC 1563039 (**1**) 1563041 (**2**).

Acknowledgements

The Authors thank The Tunisian Ministry of Higher Education and Scientific Research for the financial support. M. H. is grateful to Professor Taha Guerfel for the helpful discussions.

References

[1] a) J.T. Groves, P. Viski, J. Org Chem. 55 (1990) 3628-3634; b) J.T. Groves, P. Viski, J. Am. Chem. Soc. 111 (1989) 8537-8538.

[2] T.L. Stuk, P.A. Grieco, M. Marsh, J. Org. Chem. 56 (1991) 2957-2959.

[3] a) J.T. Groves, T.E. Nemo, R.S. Myers, J. Am. Chem. Soc.101 (1979) 1032-1033; b) J.T. Groves, T.E. Nemo, J. Am. Chem. Soc.105 (1983) 5786-5791.

[4] N. Amiri, P. Maux, H. Srour, H. Nasri, G. Simonneaux, Tetrahedron 70 (2014) 8836-8842.

[5] K. Kalyanasundaram, Photochemistry of Polypyridine and Porphyrin Complexes, Academic Press, San Diego, 1992.

[6] a) J. Simon, J.J. Andre, Molecular Semiconductors, Springer, Berlin, 1985; b) A.W. Nevin, G.A. Chamberlain, J. Appl. Phys. 69 (1991) 4324-4332.

[7] A. Policard, A. Leuller, Compt. Rend. Soc. Wood 91 (1924) 1423-1424.

[8] F. Megnin, P.J. FaustinoLyon, R.C. Lelkes, P.I. Cohen, Biochim. Biophys. Acta 929 (1987) 173-181.

[9] S. Nakajima, T. Takemura, I. Sakata, Cancer Letters 92 (1995) 113-118.

[10] A. N. Vzorov, D. W. Dixon, J. S. Trommel, L. G. Marzilli, R. W. Compans, Antimicrob. Agents and Chemother. 46 (2002) 3917-3925.

[11] V. Car, O. Gaud, I. Sylvain, O. Bow-don, M. Spiro, J. Blais, R. Granet, P. Kraus, M. Guilloton, J. Photochem. Photobiol. B*: Biol*. 48 (1999) 57.

[12] E. Reddi, M. Ceccon, G. Valduga, G. Jori, J. C. Bommer, F. Elisei, L. Latterini, U. Mazzucato, Photochemistry and Photobiology. 75 (2002**)** 462-470.

[13] K. G. Yu, D. H. Li, Ch. H. Zhou, J. L. Diao, Chinese Chemical Letters. 20 (2009) 411.

[14] J. Ramesh, S. Sujatha, C. Arunkumar, RSC Adv., DOI: 10.1039/C6RA09148B.

[15] A. Mansour, M. Zaied, I. Ali, S. Soliman, M. Othmani, Polyhedron. 127 (2017) 496-504.

[16] G. D. Bajju, G. Devi, S. Katoch, M. Bhagat, Deepmala, Ashu, S. Kundan, S. K. Anand, Bioinorg Chem and App. 2013 http://dx.doi.org/10.1155/2013/903616

[17] E. Maligaspe, T. Kumpulainen, H. Lemmetyinen, N. V. Tkachenko, N. K. Subbaiyan, M. E. Zandler, F. D'Souza, J. Phys. Chem. A. 114 (2010) 268–277

[18] N. Amiri, S. Nasri, T. Roisnel, G. Simonneaux, H, Nasri, Acta Crystallogr. E 71 (2015) 73-74.

[19] H. Toumi, N. Amiri, M. S. Belkhiria, J.C. Daran, H. Nasri, Acta Crystallogr. 68 (2012) 1557-1558.

[20] A. Mansour, Y. Belghith, M.S. Belkhiria, A. Bujacz, V. Guerineau, H. Nasri, J. Porph. Phthalocya. 17 (2013) 1094-1103.

[21] M.A. Spackman, D. Jayatilaka, CrystEngComm 11 (2009) 19-32.

[22] J.J. McKinnon, M.A. Spackman, A.S. Mitchell, Acta Cryst. B 60 (2004) 627-668.

[23] M.A. Spackman, J.J. McKinnon, D. Jayatilaka, CrystEngComm 10 (2008) 377-388.

[24] M.J. Turner, J.J. McKinnon, D. Jayatilaka, M.A. Spackman, CrystEngComm 13 (2011) 1804-1813

[25] A.Y. Meyer, Chem. Soc. Rev. 15 (1986) 449–474.

[26] J. Rudnick, G. Gaspari, J. Phys. A: Math. Gen. 19 (1986) L191–L193.

[27] A. Baumgärtner, J. Chem. Phys. 99 (1993) 7496–7501.

[28] J.J Koenderink, Solid Shape, Cambridge MA, MIT Press, 1990.

[29] J.J Koenderink, A.J Van Doorn, Image and Vision Computing 10 (1992) 557-564.

[30] S.K. Wolff, D.J. Grimwood, J.J. McKinnon, M.J. Turner, D. Jayatilaka, M.A. Spackman, CrystalExplorer Version 3.1**,** University of Western Australia, 2012.

[31] M.A. Spackman, J.J. McKinnon, CrystEngComm 4 (2002) 378-392.

[32] J.J. McKinnon, D. Jayatilaka, M. A. Spackman, Chem. Commun. 37 (2007) 3814-3816.

[33] D. Jayatilaka, D.J. Grimwood, Computational Science – ICCS 4 (2003) 142-151.

[34] D. Jayatilaka, D.J. Grimwood, A. Lee A. et al., Tonto, A System for Computational Chemistry, the University of Western Australia, Nedlands, Australia, 2005.

[35] D.D. Perrin, W.L.F. Armarego, Purification of Organic Solvents, Pergamon Press, Oxford, 1988.

[36] J.S. Lindsey, H.C. Hsu, I.C. Schreiman, Tetrahedron Letters 27 (1986) 4969-4970.

[37] K.M. Smith, Porphyrins and Metalloporphyrins, Elsevier: Amsterdam, The Netherlands, 1975.

[38] M.C. Burla, R. Caliandro, M. Camalli, B. Carrozzini, G.L. Cascarano, L.De Caro, C. Giacovazzo, G. Polidori, R. Spagna, SIR2004: an improved tool for crystal structure determination and refinement, J. Appl. Cryst. 38 (2005) 381-388.

[39] G.M. Sheldrick, Acta Cryst. A64 (2008) 112-122.

[40] P.J. Becker, P. Coppens, Acta Crystallogr. A30 (1974) 129-147.

[41] M.J. Frisch, G.W. Trucks, H.B. Schlegel et al., GAUSSIAN 09 Revision A.1, Gaussian, Inc., Wallingford CT, 2009.

[42] R. Dennington, T. Keith, J. Millam, GAUSSVIEW VERSION 5, Semichem Inc Shawnee Mission KS, 2009.

[43] L.E. Roy, P.J. Hay, R.L. Martin, J. Chem. Theory Comput. 4 (2008) 1029-1031.

[44] C. Liu, D. Zhang., M. Gao, S. Liu., Chem. Res. Chinese Universities 31 (2015) 597-602.

[45] K. Ezzayani, A.B. Khelifa, E. Saint-Aman, F. Loiseau, H. Nasri, J. Mol. Structure 2017. DOI : 10.1016/j.molstruc.2017.02.054.

[46] V. McKee, C.C. Ong, G.A. Rodley. Inorg. Chem. 23 (1984) 4242-4248.

[47] Papers", **175th** National Meeting **of** the American Chemical Society, Anaheim, CA, March 1974; American Chemical Society: Washington, DC, 1978; INOR 15. Hoard, J. L., private communication.

[48] S.A. Ikbal, S. Brahma, S. P. Rath, Inorg. Chem. 51 (2012) 9666-9676.

[49] M. Vinodu, I. Goldberg, New J. Chem. 28 (2004) 1250-1254.

[50] D.V. Konarev, S.S. Khasanov, A. Otsuka, G. Saito, R.N. Lyubovskaya, Inorg Chem. 46 (2007) 2261-2271.

[51] K. Ezzayani, Z. Denden, E. Saint-Aman, N. Najmudin, F. FLoiseau, H. Nasri, Eur. J. Inorg. Chem. 31 (2014) 5348-5361.

[52] L. Jiang, R.A. Zaenglein, J.T. Engle, C. Mittal, C.S. Hartley, C.J. Ziegler, H. Wang, Chem. Commun. 48 (2012) 6927-6929.

[53] K. Ezzayani, A.B. Khelifa, E. Saint-Aman, F. Loiseau, H. Nasri, Polyhedron 117 (2016) 817-825.

[54] I. Fleming, Frontier Orbitals and Organic Chemical Reactions, John Wiley and Sons, New York, 1976.

[55] K. Fukui, Science 218 (1982) 747-754.

[56] L. Padmaja, C. Ravikumar, D. Sajan, I.H. Joe, V.S. Jayakumar, G.R. Pettit, O.F. Nielsen, J. Raman Spectrosc. 40 (2009) 419-428.

[57] C. Ravikumar, I.H. Joe, V.S. Jayakumar, Chem. Phys. Lett. 460 (2008) 552-558.

[58] M. Hoffman, S. Martin, W. Choi, D. Bahnemann, Chem. Rev. 95 (1995) 69-96.

[59] S. Wang, J. Li, J. Solid State Chem. 224 (2015) 40-44.

[60] Y. Kessentini, A.B. Ahmed, S.S. Al-Juaid, T. Mhiri, Z. Elaoud, Optical Materials 53 (2016) 101-108.

[61] C. Lan, S. Zhao, T. Xu, J. Ma, S. Hayase, T. Ma, J. Alloy. Compd. 655 (2016) 208–214.

[62] Y. Mikami-Terao, M. Akiyama, Y. Yuza, T. Yanagisawa, O. Yamada, T. Kawano, M. Agawa, H. Ida, H. Yamada, Experimental Eye Research 89 (2009) 200-208.

[63] J.-W. Li, Z.-M. Wu, D. Magetic, L.-J. Zhang, Z.-L. Chen, Tumor Biol. 36 (2015) 9685-9692.

[64] S. Asayama, E. Kawamura, S. Nagaoka, H. Kawakami, Molecular Pharmaceutics 3 (2006) 468-470.

[65] A. Mahdhi, M. Ángeles Esteban, Z. Hmila, K. Bekir, F. Kamoun, A. Bakhrouf, B. Krifi, Artemia culture 39 (2012) 1151-1159.

[66] F. R. Kooriyaden, S. Sujatha, C. Arunkumar**,** Polyhedron. 2017, https://doi.org/10.1016/j.poly.2017.03.002

[67] F.R. Kooriyaden, S. Sujatha, C. Arunkumar, Polyhedron 97 (2015) 66-74.

[68] A. Mansour, M. Zaied, I. Ali, S. Soliman, M. Othmani, Polyhedron 127 (2017) 496-504.

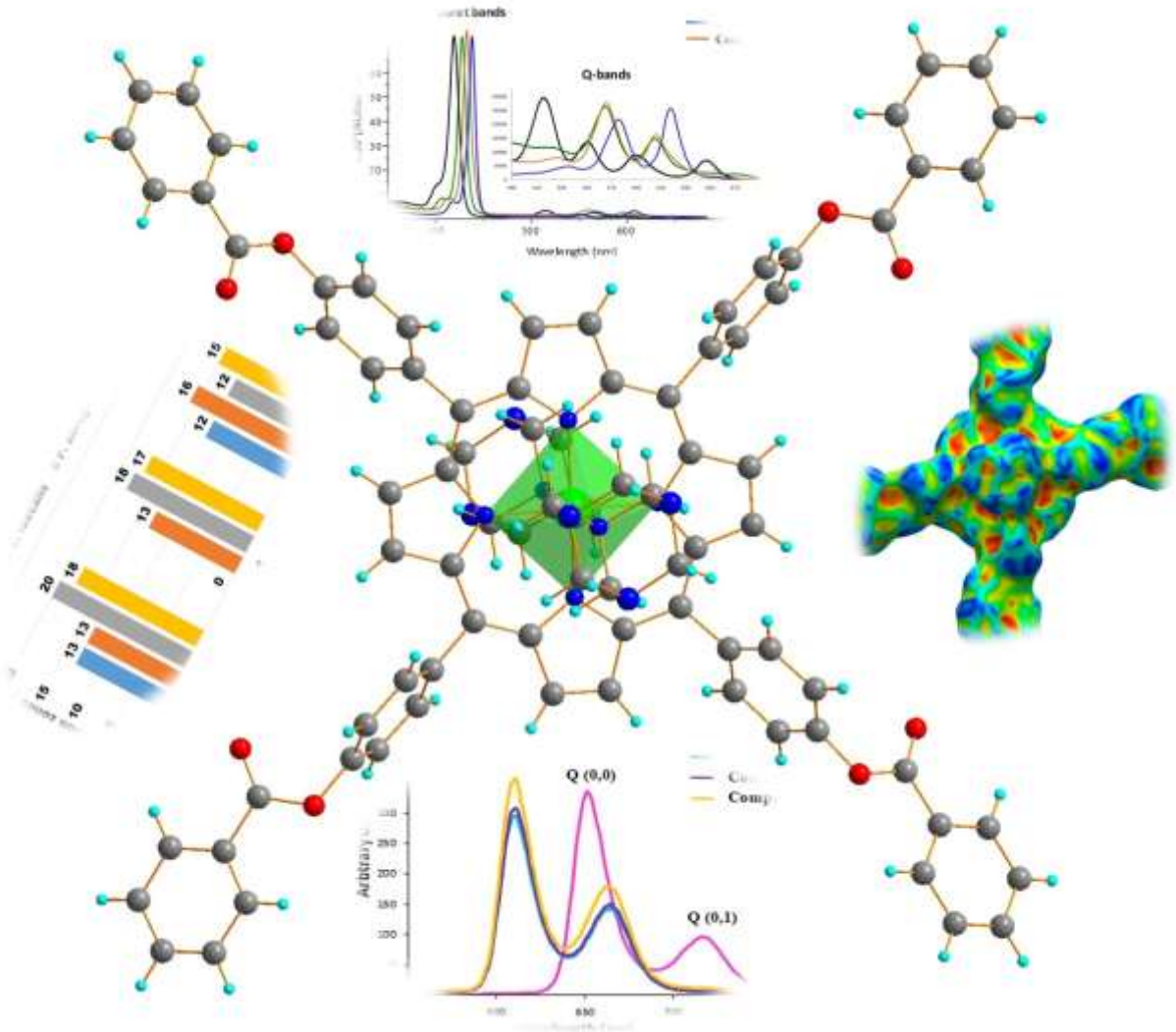

- ✓ Two novel magnesium(II)tetraphenylporphyrin-based six-coordinate complexes were synthesized.
- ✓ Structures were determined by X-Ray diffraction technique and quantitatively elucidated using Hirshfeld surface approach.
- ✓ UV-visible and Fluorescence investigations were made.
- ✓ HOMO-LUMO energy gap was modelled using DFT approach.
- ✓ Role of our complexes as novel antibacterial agents was also performed.